DOI:10.1190/segam2020-3420041.1

Stress paths and predicted time-shifts around a depleting reservoir

Hong Yan (NTNU), Audun Bakk (SINTEF), Rune M. Holt (NTNU), Serhii Lozovyi (SINTEF)*

Summary

Time-lapse (4D) seismic is an essential tool for monitoring the subsurface in and around producing hydrocarbon or CO_2 storage reservoirs. The seismic time-shifts, in the reservoir as well as in the overburden, depend on the stress changes and strains induced by the subsurface depletion or the inflation. In this study, geomechanical modeling is used to quantify the stress changes and strains in a synthetic model for the formations in and around a depleting reservoir. The estimated strains are coupled to experimentally determined strain sensitivities for P-wave velocities of shales, to predict time-shifts in the surroundings of the reservoir. The modeling shows that the stiffness contrast between the reservoir and its surroundings plays an important role in controlling the stress and strain changes in the subsurface. The strain sensitivity of the vertical P-wave velocity in the surroundings is significant and is rapidly increasing in magnitude with the proximity to the reservoir. Correspondingly, the time-shifts are increasing with depth in the overburden and decreasing with depth in the underburden. In this study, the time-shifts of the surroundings are changing most between the depths corresponding to one and two reservoir radii above and below the reservoir.

Introduction

The time-shifts in the overburden, induced by a depleting reservoir, turn out to be significant in comparison with time-shifts in the reservoir (Hall *et al.*, 2002). This means that proper monitoring of the reservoir needs to account for the changing overburden. The time-shift signals in the reservoir are normally affected by several factors, including saturation and pore pressure changes, in addition to possible temperature changes caused by water injection (Landrø, 2002). However, the overburden time-shifts are purely due to the geomechanical changes linked to the pore pressure change in the reservoir. Thus, the overburden is very useful for direct quantification of stress alterations and strains (Bakk *et al*., 2019; Røste *et al*., 2007).

Production related reservoir depletion and compaction problems can be studied by geomechanical simulations (modeling). The vertical and horizontal stress changes, within and outside the reservoir, can be quantified by the arching coefficient γ_v and the depletion coefficient γ_h (Hettema *et al.*, 2000):

$$\gamma_v = \frac{\Delta\sigma_v}{\Delta P_{res}};\ \gamma_h = \frac{\Delta\sigma_h}{\Delta P_{res}}, \qquad (1)$$

where $\Delta\sigma_v$ and $\Delta\sigma_h$ are the vertical and the horizontal stress changes, respectively, caused by the pore pressure change within the reservoir (ΔP_{res}). Compressive stresses are defined as positive. These coefficients provide an efficient way to evaluate the stress changes related to the pore pressure change in the reservoir. Rudnicki (1999) studied stress changes in reservoirs using an analytic model for an ellipsoid-shaped reservoir that allows for elastic contrast between the reservoir and the surroundings. Since this model neglects the zero-stress free surface effect, it is in practice restricted to ellipsoidal reservoirs at depths larger than the reservoir diameter (Fjær *et al.*, 2008). In contrast, Geertsma (1973) introduced the nucleus of the strain model, which accounts for the free surface although no elastic contrast is permitted between the reservoir and the surroundings. This model was used to study subsidence from compaction, i.e. focusing on the rocks surrounding the reservoir. Analytical models may be useful as a qualitative screening tool, but numerical simulations are needed to grasp more realistic scenarios to obtain relevant quantitative data.

To fully utilize the potential of 4D seismic inversion, the geomechanical data may be further constrained by dedicated laboratory studies, from where the static and dynamic properties for a variety of stress variations may be obtained (Holt *et al.*, 2018). In this respect, the stress-path ratio κ is a convenient parameter. The stress path ratio for the reservoir (κ_{res}) quantifies the relative change between the effective horizontal $\Delta\sigma'_h$ and vertical stress changes $\Delta\sigma'_v$ (Fjær *et al*., 2008), respectively (cf. equation (2)). However, in the surroundings the pore pressure change is usually not accessible, whereas the total stress changes may be estimated from advanced geomechanical modelling using realistic rock physical properties as an input. Thus, the stress-path ratio for the surroundings (κ_{sur}) is defined as the ratio between the total horizontal $\Delta\sigma_h$ and the total vertical $\Delta\sigma_v$ stress change (Holt *et al.*, 2018), respectively:

$$\kappa_{res} = \frac{\Delta\sigma'_h}{\Delta\sigma'_v} = \frac{\gamma_h - \alpha}{\gamma_v - \alpha};\ \kappa_{sur} = \frac{\Delta\sigma_h}{\Delta\sigma_v} = \frac{\gamma_h}{\gamma_v}, \qquad (2)$$

where the Biot coefficient (α) is conveniently assumed to be equal to 1. In the case of no elastic contrast between the reservoir and the surroundings, cf. the model of Geertsma (1973), the surroundings maintain approximately a constant mean stress in the space not influenced by the free surface (Fjær *et al*., 2008), i.e., $\gamma_v + 2\gamma_h \approx 0$.

Previous studies of the stress-path dependence using numerical geomechanical modeling have often considered the stress development primarily inside and to a lesser extent outside of the reservoir (Mahi, 2003; Mulders, 2003).

10.1190/segam2020-3420041.1

Though, stress paths of the overburden also are considered in some works (Herwanger and Horne, 2009). Here we will mostly consider the surroundings of the reservoir.

Holt *et al.* (2018) examined the stress path dependence of ultrasonic velocities. A stress sensitivity parameter for the vertical P-wave velocity (V_{Pv}) is defined:

$$S_v = \frac{\Delta V_{Pv}}{V_{Pv}\Delta\sigma_v} = \frac{a}{3} + b - A_s B_s c + \left[\frac{2a}{3} - b - B_s(1-A_s)c\right]\kappa, \quad (3)$$

where the linear parameters *a*, *b*, and *c* are experimentally determined from laboratory field core measurements. The A_s and the B_s are the Skempton parameters, controlling pore pressure changes during undrained loading (Skempton, 1954). The corresponding strain sensitivity parameter R_v for the V_{Pv} is given by:

$$R_v = \frac{\Delta V_{Pv}}{V_{Pv}\Delta\varepsilon_v} = S_v M_v, \text{ where } M_v = \frac{\Delta\sigma_v}{\Delta\varepsilon_v}. \quad (4)$$

Notice that the generalized stiffness M_v depends strongly on stress path. The relative change in the vertical two-way travel time (TWT) (Hatchell and Bourne, 2005; Røste *et al.*, 2005) can be calculated by:

$$\frac{\Delta\text{TWT}}{\text{TWT}} = -(1+R_v)\Delta\varepsilon_v, \quad (5)$$

where $\Delta\varepsilon_v$ denotes the axial strain that is defined positive for compaction. Since the R_v in practice varies in the subsurface, the relative time-shift in equation (5) represents a local quantity that is termed time-strain in the literature (Hodgson *et al.*, 2007). To account for the variability of the strain sensitivity, the true time-shift must be calculated as a sum (integral) along the ray-path. In our study, we will discuss the behavior of these stress and strain-dependent quantities for different properties of the surroundings.

Geomechanical modeling

We consider a disk-shaped reservoir (cf. Figure 1). The numerical simulations are performed with a finite element software (DIANA). An axisymmetric model is defined to save computation time and to allow computations with sufficient fine mesh. Displacements are neither permitted along the horizontal boundary (cf. Figure 1) nor at the bottom of the model (5000 m depth). The top of the model assumes a free surface. The element size is 25 m for the entire model. We further assume that the pore pressure is reduced (drained) in the reservoir from 35 MPa to 0 MPa due to the depletion. In general, there is typically a stiffness contrast between the surroundings and the reservoir. Therefore, we consider different contrasts by applying three different sets of shale properties in the surroundings based upon experimental laboratory data of shales, all differing from the reservoir properties. The estimated values of the stress sensitivity coefficients *a*, *b*, and *c* and the Skempton parameters (cf. equation (3)) for the shales are provided by Holt *et al.* (2018). All shales were brine-saturated with the expected in-situ salinity and tested at in-situ stress and pore pressure conditions. Although the shales samples are anisotropic, the current modeling is conveniently assuming isotropic rock properties. Thus, the values of the Poisson's ratios and Young's moduli refer to stress changes applied in the vertical direction, i.e. normal to the bedding plane. The Skempton parameters are obtained from static undrained tests and the stress sensitivity parameters are calibrated to ultrasonic velocity changes (Holt *et al.*, 2018). The basic rock properties for the shales and the reservoir rock are given in Table 1. The reservoir rock property is referring to a weak North-Sea reservoir sandstone (Table A.2 in Fjær *et al.* (2008)). Since the surroundings are assumed to have very low permeability, undrained moduli are used for the shales. In contrast, drained moduli are applied for the reservoir rock. In this study, we restrict the discussion to the vertical symmetry line through the center of the model.

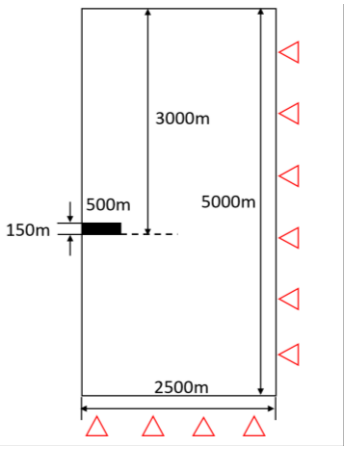

Figure 1: The half-space geomechanical model and the fixed boundaries (red triangles). The top interface is assumed free. The disk-shaped reservoir (black rectangle) has a top horizon at 2850 m, a radius of 500 m, and a thickness of 150 m.

Table 1: Rock properties for the shales and the reservoir: density (ρ), Young's modulus (E), Poisson's ratio (ν), and porosity (ϕ).

	ρ (g/cm^3)	E (GPa)	ν (-)	ϕ (%)
Shale B	2.26	5.3	0.30	24
Shale D	2.23	3.1	0.40	29
Shale M	2.01	2.3	0.39	36
Reservoir	2.20	0.4[1]	0.45[1]	30

[1]Drained property.

The numerical geomechanical modeling results (cf. Figure 2) are quantified by the stress path coefficients as given in equation (1). A contrast between the Young's moduli in the reservoir and the surroundings has a significant effect on the stress path. The γ_v is positive at all depths, implying vertical

DOI:10.1190/segam2020-3420041.1

stress reduction as a result of the depletion, and reaches the peak value near the upper and lower bounds of the reservoir. Moreover, the arching effect is increasing with the surrounding rock-stiffness. The magnitude (absolute value) of the γ_h is similarly scaling with the stiffness contrast between the reservoir and its surroundings. However, the γ_h follows qualitatively a different depth trend as compared to the γ_v. The depletion coefficient is exhibiting negative values in the shallow and deep formations away from the reservoir boundaries. In the proximity of the reservoir, the γ_h shifts polarity and becomes discontinuous at the vertical reservoir boundaries. Generally, the zone of positive γ_h is much thicker than the thickness of the reservoir. The κ_{sur} above and below the center of the reservoir becomes positive due to the shift in polarity of the γ_h.

Discussion of results

This study shows that the reservoir surroundings are significantly influenced by the reservoir depletion, as quantified by the vertical (γ_v) and the horizontal (γ_h) stress path coefficients. The stress and strain changes are most sensitive near the edges of the reservoir, where the γ_h is flipping polarity near the reservoir and finally becomes discontinuous at the horizontal reservoir boundaries (cf. Figure 2). This implies that the stress path coefficient of the surroundings (κ_{sur}) has an accompanying significant depth sensitivity. All Young's modulus contrasts we have tested are significant (cf. Table 2), and consequently, cause the flip of polarity in the γ_h from approximately 350 m above and below the reservoir. The latter may lead to drilling problems as the stress gradient becomes very large (Ditlevsen *et al.*, 2018). The variation range of κ_{sur} implies that the stress state in the overburden is going from a (close to) constant mean stress state (κ_{sur} = -0.5) at shallow depths, through a triaxial stress state (κ_{sur} = 0) closer to the reservoir, and positive values at the reservoir boundary approaching uniaxial strain (K_0). The latter is typical for a relatively stiff overburden (Morita & Fuh, 2009). This depth trend is quantitatively mirrored through the underburden. However, it is not a perfect symmetry with respect to these quantities around the reservoir (overburden vs. underburden) since the free surface at the top of the model is opposed by a rigid boundary at the bottom of the model. The largest magnitude of κ_{sur} appears for the B shale, which is the stiffest of the shales.

The stress state in the reservoir is between a K_0 and isotropic stress changes (note that κ_{res} refers to the effective stress path coefficients cf. equation (2)). The sensitivity study by Mulders (2003) also shows that both contrasts (reservoir vs. surroundings) in the Young's moduli and the Poisson's ratios will promote stress concentrations. The Young's modulus contrast seems to be most influential in this respect.

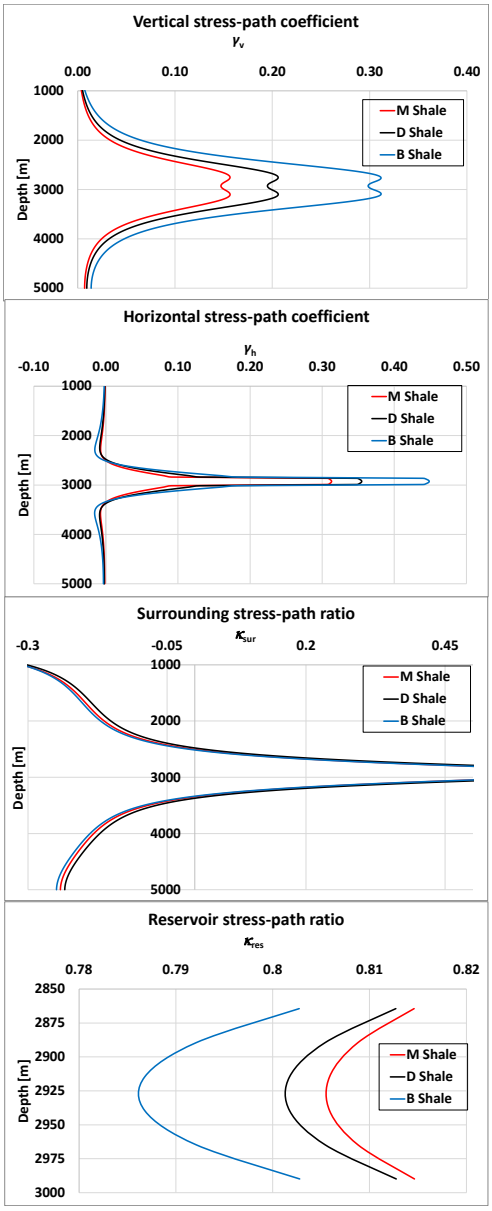

Figure 2: Geomechanical simulation results for the vertical (γ_v) and horizontal (γ_h) stress path coefficients cf. equation (1), and the stress path ratios for the surroundings (κ_{sur}) and the reservoir (κ_{res}) cf. equation (2)), quantified along a vertical line through the center of the reservoir.

The output of the geomechanical modeling together with the experimental data on the stress sensitivities were used to predict the relative time-shifts by combining equations (3), (4) and (5). The stress sensitivity (S_v), the strain sensitivity (R_v), and the relative two-way time-shift (ΔTWT/TWT) show all a strong depth-dependence (cf. Figure 3). The

10.1190/segam2020-3420041.1

magnitudes of the strain sensitivity and the relative two-way time-shift are highest when Young's modulus contrast is highest (B shale). The D and M shales, with similar Young's moduli and Poisson's ratio contrasts (cf. Table 2), show similar strain sensitivity and relative time-shifts. Notably, the relative time-shifts in the surroundings are significant.

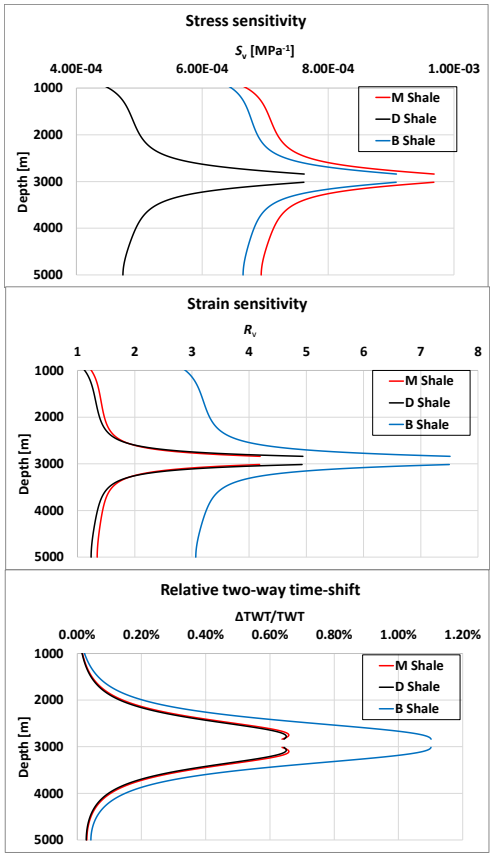

Figure 3: Geomechanical simulation results for the stress sensitivity parameter S_v (cf. equation (3)), the strain sensitivity parameter R_v (cf. equation (4)) and the relative two-way vertical travel time-shift (time-strain) ΔTWT/TWT (cf. equation (5)), quantified along a vertical line through the center of the reservoir.

The vertical strain sensitivity of the P-wave velocity of the surroundings is depth-dependent and is rapidly changing when the reservoir boundary is approached (cf. Figure 3). Such variability in the surroundings (overburden) is even more pronounced for an overburden consisting of several layers with contrasting stiffnesses. The 4D seismic data of De Gennaro *et al.* (2008) from the overburden of the Elgin and Franklin fields exhibit a significant and non-monotone trend of the *R*-factor, particularly pronounced in the stiff chalk layers above the cap-rock. Even though more and more studies now regard the *R*-factor as a spatially variable, it has in many cases been treated as constant for larger stretches and even the entire overburden (cf. references in MacBeth *et al.* (2018)). An "average" *R* for the entire overburden may be calculated for the comparison to the values reported in the literature (cf. Table 2). The "average" overburden *R*-factor around the reservoir tends to increase with increasing stiffness contrast between the reservoir and the surroundings. This trend is also reflected in the corresponding trend of the relative time-shifts, calculated by applying these "average" *R*-factors into equation (5) (equivalent to the true time-shift as the model elements have equal thicknesses). The small magnitude of the *R* (from 1.9 to 4.2) for our case are reflecting pronounced shear-stress changes, which implies significantly lower strain sensitivities than, e.g., isotropic stress changes (Holt *et al.*, 2018). These values are in line with the overburden *R*-factors reported from field data (cf. Table 1 in MacBeth *et al.*, 2018). This underlines the importance of properly calibrated rock-physics models to constrain the 4D seismic analysis.

Table 2: Young's modulus contrast (E_{sur}/E_{res}) and Poisson's ratio contrast (ν_{sur}/ν_{res}) between the reservoir and the surroundings, the "average" *R*-factor for the entire overburden and the relative time-shift.

	E_{sur}/E_{res} (-)	ν_{sur}/ν_{res} (-)	R (-)	ΔTWT/TWT (%)
B Shale	13.25	0.67	4.16	0.22
D Shale	7.75	0.89	1.93	0.14
M Shale	5.75	0.87	1.92	0.15

Conclusion

Finite element simulations are used to study a synthetic case consisting of a disk-shaped depleting reservoir surrounded by shales, which are probed with different geomechanical properties. These data are converted to strain sensitivities and time-shifts in the reservoir's surroundings (overburden) by using laboratory data. The geomechanical modeling shows that the stiffness contrast between the reservoir and its surroundings plays an important role in controlling the stress path coefficients. A significant contrast in stiffness will strongly affect the value and polarity of the horizontal stress path coefficient. The stress path is very sensitive to the depth when the reservoir boundaries are approached. By coupling geomechanical simulations to a calibrated rock-physics model for the stress and strain sensitivities of the velocities, 4D seismic data may be appropriately inverted for stress changes and strains – for efficient and safe production.

Acknowledgments

We thank the Research Council of Norway through the PETROMAKS-2 program (Grant 294369), AkerBP, Equinor and Shell for funding in the project: *Improved prediction of stress and pore-pressure changes in the overburden for infill drilling.*

REFERENCES

Bakk, A., R. M. Holt, A. Bauer, B. Dupuy, and A. Romdhane, 2019, Offset-dependent overburden time- shifts from ultrasonic data: 81st EAGE Conference and Exhibition, Expanded Abstracts, Tu-R02-13.

De Gennaro, S., A. Onaisi, A. Grandi, L. Ben-Brahim, and V. Neillo, 2008, 4D reservoir geomechanics: a case study from the HP/HT reservoirs of the Elgin and Franklin fields: First Break, **26**, 53–59, doi: https://doi.org/10.3997/1365-2397.2008019.

Ditlevsen, F., F. Bourgeois, and M. Calvert, 2018, Handling wellbore instability in overburden Tertiary shales: 80th EAGE Conference and Exhibition, Expanded Abstracts, Tu-C-07.

Fjær, E., R. M. Holt, P. Horsrud, A. M. Raaen, and R. Risnes, 2008, Petroleum related rock mechanics: Elsevier.

Geertsma, J., 1973, A basic theory of subsidence due to reservoir compaction: The homogeneous case: Verhandelingen van het Koninklijk Nederlands Geologisch Mijnbouwkundig Genootschap, **28**, 43–62.

Hall, S. A., C. MacBeth, O. I. Barkved, and P. Wild, 2002, Time-lapse seismic monitoring of compaction and subsidence at Valhall through cross-matching and interpreted warping of 3D streamer and OBC data: 72nd SEG Annual Meeting, Expanded Abstracts, 1696–1699.

Hatchell, P., and S. Bourne, 2005, Rocks under strain: Strain-induced time-lapse time shifts are observed for depleting reservoirs: The Leading Edge, **24**, 1222–1225, doi: https://doi.org/10.1190/1.2149624.

Herwanger, J. V. and S. A. Horne, 2009, Linking reservoir geomechanics and time-lapse seismics: Predicting anisotropic velocity changes and seismic attributes: Geophysics, **74**, no. 4, W13–W33, doi: https://doi.org/10.1190/1.3122407.

Hettema, M. H. H., P. M. T. M. Schutjens, B. J. M. Verboom, and H. J. Gussinklo, 2000, Production-induced compaction of a sandstone reservoir: The strong influence of stress path: SPE Reservoir Evaluation and Engineering, **3**, 342–347, doi: https://doi.org/10.2118/65410-PA.

Hodgson, N., C. MacBeth, L. Duranti, J. Rickett, and K. Nihei, 2007, Inverting for reservoir pressure change using time-lapse time strain: Application to Genesis Field, Gulf of Mexico: The Leading Edge, **26**, 649–652, doi: https://doi.org/10.1190/1.2737104.

Holt, R. M., A. Bauer, and A. Bakk, 2018, Stress-path-dependent velocities in shales: Impact on 4D seismic interpretation: Geophysics, **83**, no. 6, MR353–MR367, doi: https://doi.org/10.1190/geo2017-0652.1.

Landrø, M., 2002, Uncertainties in quantitative time-lapse seismic analysis: Geophysical Prospecting, **50**, 527–538.

MacBeth, C., A. Kudarova, and P. J. Hatchell, 2018, A semi-empirical model of strain sensitivity for 4D seismic interpretation: Geophysical Prospecting, **66**, 1327–1348, doi: https://doi.org/10.1111/1365-2478.12648.

Mahi, A., 2003, Stress path of depleting reservoirs: M.S. thesis, NTNU.

Morita, N., and G.-F. Fuh, 2009, Parametric analysis of stress reduction in the caprock above compacting reservoirs: SPE Drilling and Completion, **24**, 659–670, doi: https://doi.org/10.2118/114629-PA.

Mulders, F. M. M., 2003, Modeling of stress development and fault slip in and around a producing gas reservoir: Ph.D. thesis, TU Delft.

Røste, T., A. Stovas, and M. Landrø, 2005, Estimation of layer thickness and velocity changes using 4D prestack seismic data: 67th EAGE Conference and Exhibition, Expanded Abstracts, C010.

Røste, T., M. Landrø, and P. Hatchell, 2007, Monitoring overburden layer changes and fault movements from time- lapse seismic data on the Valhall Field: Geophysical Journal International, **170**, 1100–1118, doi: https://doi.org/10.1111/j.1365-246X.2007.03369.x.

Rudnicki, J. W., 1999, Alteration of regional stress by reservoirs and other inhomogeneities: stabilizing or destabilizing?: 9th ISRM Congress. International Society for Rock Mechanics and Rock Engineering.

Skempton, A. W., 1954, The pore-pressure coefficients A and B: Géotechnique, **4**, 143–147, doi: https://doi.org/10.1680/geot.1954.4.4.143.